Analyst

COMMUNICATION

View Article Online
View Journal | View Issue

Cite this: *Analyst*, 2014, **139**, 5069

Received 21st February 2014
Accepted 6th August 2014

DOI: 10.1039/c4an00371c

www.rsc.org/analyst

Label-free *in vitro* visualization of particle uptake into human oral buccal epithelial cells by confocal Raman microscopy†

B. Kann,[a] B. J. Teubl,[ab] E. Roblegg[bc] and M. Windbergs*[ade]

In this study, we present confocal Raman microscopy for chemically selective analysis of a human buccal epithelial cell layer with a focus on label-free visualization of particle uptake into the cells. We demonstrate the suitability and benefit of this analytical technique in comparison to confocal fluorescence microscopy for three dimensional imaging of *in vitro* cell models.

The uptake of small particles into the human body has become of major interest in various areas of research. This trend is not only due to the increasing attempt to develop novel nano-sized particulate therapeutics for targeted medical application of drugs. In addition, particles in the nano- and micrometer size range are to an increasing degree incorporated in various consumer products like tooth paste and cosmetics, and are also used as food additives.[1–7] Thus, profound scientific knowledge about the fate of such particles in the human body is mandatory to estimate absorption and potential toxicological effects.

In this context, titanium dioxide (TiO_2), a white, inorganic, crystalline compound plays an important role, as this substance is frequently used as white pigment in paint and plastic, sunscreen, tablets, chewing gum and as food additive.[1,8] Due to the prevalent use of TiO_2, the Organization for Economic Co-operation and Development (OECD) listed TiO_2 as priority nanomaterial to analyze the fate upon contact with the human body.[9]

Most products containing TiO_2 are regularly or spuriously taken up *via* the oral route. Consequently, the buccal mucosa is the first site of contact, where these particles may be absorbed into the human body. Thus, studying the interaction of TiO_2 particles with this biological barrier is of high relevance.

Excised porcine buccal mucosa is a common system for *in vitro* studies simulating the human mucosa quite accurately.[10,11] However, due to limited tissue access, a cell culture-based model using a human oral epithelial cell line has successfully been established as an alternative *in vitro* system.[12–14] Furthermore, the suitability to study nanoparticle uptake into this buccal *in vitro* model has been demonstrated.[14] However, adequate analysis of such systems is challenging.

In this context, the combination of spectroscopic and microscopic techniques is a valuable analytical approach to investigate cells or tissue on the subcellular level as well as to analyze cellular internalization of particulate systems. In this field, fluorescence microscopy is currently the most applied spectroscopic technique. For selective fluorescence detection, the structure of interest is labeled with a selective marker molecule prior to investigation. However, these marker molecules are often prone to photobleaching, limiting the time span for fluorescence microscopy analysis. Furthermore, due to linkage of the marker substance to a compound of the particulate system or a cellular structure, the physicochemical properties of the sample molecule might be altered. Thus, the observed analytical results may not represent the native situation of the sample.

Recently, confocal Raman microscopy has gained increasing impact as an alternative analytical method for biomedical imaging[15–18] and specific cellular investigations[19,20] including uptake studies of diverse particulate systems.[21–26] For confocal Raman microscopy, the sample is irradiated with laser light. The frequency shift between incident and scattered light due to the interaction of photons and sample molecules is detected. Thus, non-destructive component identification within a sample can be performed by detecting the individual Raman scattering patterns serving as a molecular fingerprint.

[a]*Saarland University, Department of Biopharmaceutics and Pharmaceutical Technology, Campus A4.1, 66123 Saarbruecken, Germany. E-mail: m.windbergs@mx.uni-saarland.de*

[b]*University of Graz, Institute of Pharmaceutical Sciences, Department of Pharmaceutical Technology, Humboldtstrasse 46, 8010 Graz, Austria*

[c]*Research Center Pharmaceutical Engineering GmbH, Inffeldgasse 13, 8010 Graz, Austria*

[d]*Helmholtz Centre for Infection Research and Helmholtz-Institute for Pharmaceutical Research Saarland, Department of Drug Delivery, Campus A4.1, 66123 Saarbruecken, Germany*

[e]*PharmBioTec GmbH, Department of Drug Delivery, Campus C2.2, 66123 Saarbruecken, Germany*

† Electronic supplementary information (ESI) available. See DOI: 10.1039/c4an00371c

Consequently, the technique operates label-free and chemically selective, thus providing a promising and complimentary alternative to confocal fluorescence microscopy.

In this study, we present a non-destructive analysis of TiO_2 particles interacting with oral buccal epithelium by confocal Raman microscopy. First, we image an oral buccal epithelial cell layer discriminating cell nucleus from cell body based on the chemically selective Raman spectra of the different cellular structures. Raman microscopy images are compared to fluorescence microscopy images. In subsequent experiments, the uptake of well-characterized TiO_2 particles into oral buccal cells is visualized by confocal Raman microscopy exploiting all three spatial dimensions. Lateral images are acquired for particle localization within the cell layer, whereas vertical cross section images prove particle internalization.

For profound, label-free analysis of TiO_2 particle internalization into buccal epithelial cells by confocal Raman microscopy, a sophisticated spectroscopic investigation of the cells is initially required. Here, scattering patterns of diverse molecular structures deriving from the individual chemical composition of different cellular compartments are identified, which will later allow not only for potential internalization studies but also for TiO_2 localization within the cells. This analytical capability can be of high importance as the potential invasion of TiO_2 into cellular compartments such as the nucleus might be a concern regarding genotoxicity.

For this study, oral epithelial TR146 cells (Imperial Cancer Research Technology, London, UK) were grown in DMEM with supplements of 10% FBS, 200 μM L-glutamine, 100 IU ml^{-1} penicillin and 100 μg ml^{-1} streptomycin maintaining standard culture conditions. Sub-cultivation was performed weekly with 0.25% trypsin–EDTA. Passages 9–20 were used for experiments.

Single Raman spectra recorded from cell nucleus (blue) and cell body (red) of the buccal epithelial cells are depicted in Fig. 1A. Despite the different origin within the cell, both spectra show a dominant peak between 2800–3020 cm^{-1}. This peak represents the prominent CH-stretch vibrations,[19] which are consistent in the respective Raman spectra throughout cellular investigations, as these molecular bonds are dominant in biological samples. The spectral region between 500–1800 cm^{-1} is generally termed as the fingerprint region, as it comprises outstanding peaks, which allow the recognition of different molecular structures. Fig. 1B depicts the Raman spectra of cell body (red) and nucleus (blue) acquired in the fingerprint region. The cell nucleus representing a major compartment is a DNA rich region, where especially phosphate groups of the DNA backbone contribute to a strong scattering activity. The respective outstanding peaks at 785, 1095 and 1575 cm^{-1} are highlighted in Fig. 1B. They derive from ring breathing modes of pyrimidine bases as well as from the symmetric stretching modes of phosphate esters in DNA[19,27] allowing spectral discrimination of the nucleus from the remaining cell body based on Raman analysis. As the focus of this study is to investigate the internalization of titanium dioxide nanoparticles and their localization to the cell nucleus, compartments other than nucleus and cytoplasm are neglected.

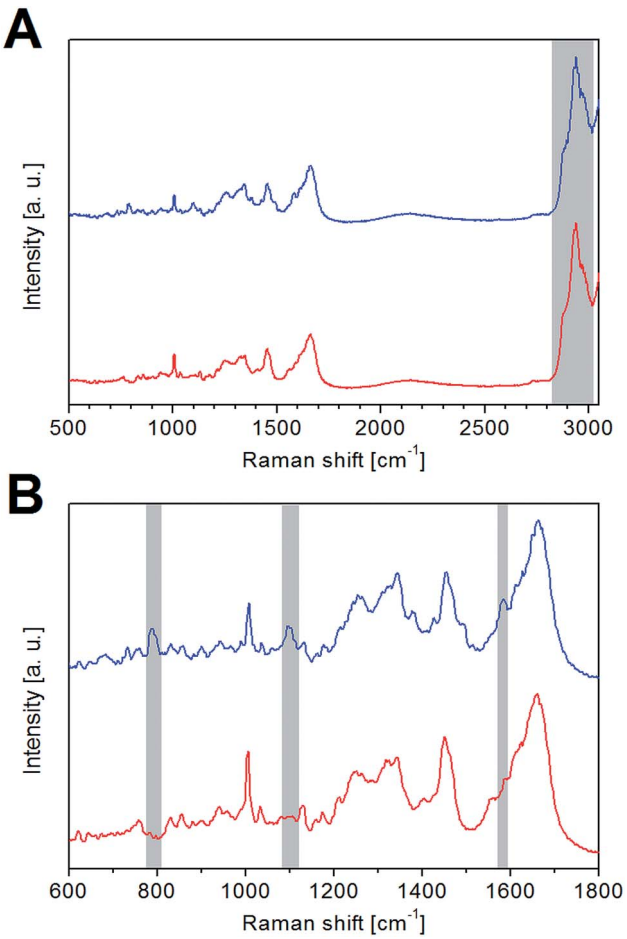

Fig. 1 Raman spectra from cell nucleus (blue) and cell body (red). (A) Overview spectra covering the entire spectral bandwidth. (B) Spectra from the fingerprint region with highlighted areas for outstanding DNA specific peaks in the nucleus spectrum.

However, literature shows that confocal Raman microscopy is suited to visualize multiple other cellular compartments.[19,20,28]

For general and quick evaluation of cultured cells with respect to morphology and confluence levels, light microscopy is the standard visualization technique used in daily cell culture lab work (Fig. 2A). However, this visual examination is only based on personal subjective observations, and therefore not suited for specified investigations.

To evaluate the potential of confocal Raman microscopy as a suitable complimentary analytical technique for cellular visualization, we performed an equally structured study with confocal fluorescence microscopy representing the current state-of-the-art technique in this field. Here, specific marker substances are used to label and consequently visualize the cellular structures of interest. Fig. 2B shows fluorescence microscopy images of a buccal epithelial cell layer (TR146) used in this study. Images were acquired with a LSM510 Meta confocal laser scanning microscope (Zeiss, Germany) through a Zeiss objective (63× magnification) with 405/BP 420–480 for the blue channel and BP 525/50 nm band pass detection for the green channel. For visual discrimination, nuclei of living cells

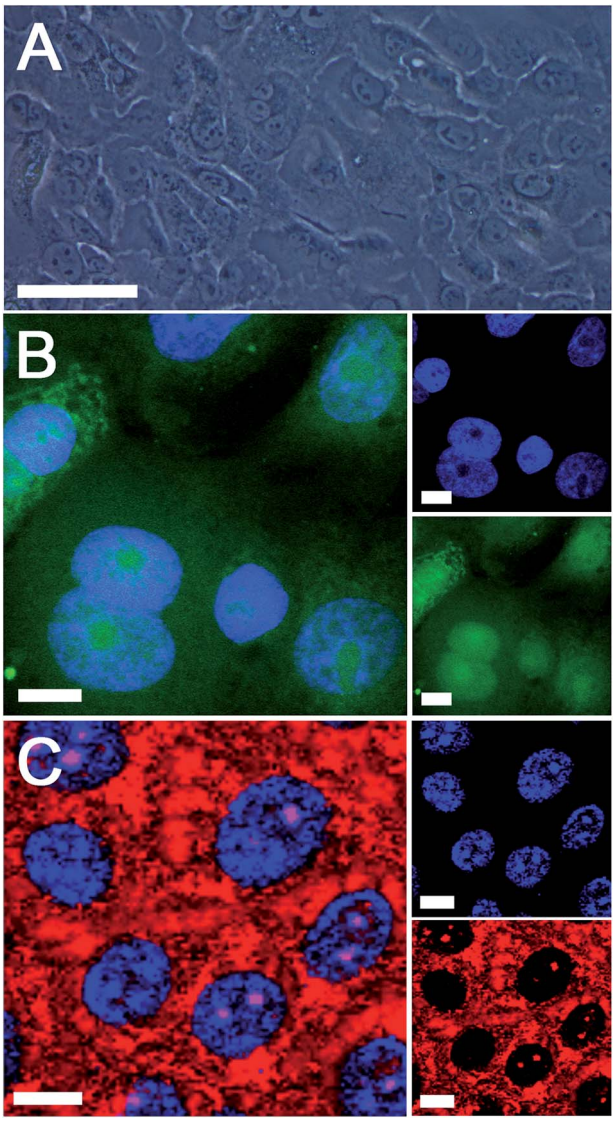

Fig. 2 Microscopic images of a buccal epithelial cell layer. (A) Light microscopy image. (B) Confocal fluorescence microscopy images showing nuclei in blue and cell bodies in green. The large panel depicts the merged image and the small panels the channel separated images. (C) Confocal Raman microscopy images visualizing nuclei in blue and cell bodies in red. The large panel shows the combined image, whereas the small panels depict the split images for each Raman signal. Scale bars are sized to 10 μm.

were stained with Hoechst 33342 (Invitrogen, Austria; 1 μg ml^{-1}), whereas the cytoplasm was stained using Calcein AM (Invitrogen, Austria; 2.5 μg ml^{-1}). Both structures are displayed in a merged fluorescence image (Fig. 2B, large panel) as well as in separate images (Fig. 2B, small panels), one showing cell nuclei (blue) the other depicting cell bodies (green). Although confocal fluorescence microscopy is successfully applied for cellular investigations, it bears several limitations. Linking marker substances to cellular structures and external particles might alter the native behavior upon interaction[29] and thus, lead to misinterpretation of analytical results. In addition, improper linkage entails loose marker molecules diffusing uncontrolled in the sample falsifying any analysis. Furthermore, the number of structures which can be visualized simultaneously is dependent on the microscopic setup, as each marker has to be irradiated by its specific absorption wavelength. Moreover, the time span for fluorescence microscopy analysis is in many cases limited, as the marker molecules are often prone to photobleaching. This results in a decrease of signal intensity or even a loss of signal as the capability of light emission of the marker molecule is destroyed over time.

In contrast, confocal Raman microscopy is a suitable complimentary technique offering the advantageous combination of label-free, chemically selective and spatially resolved analysis. Thus potential limitations of fluorescence microscopy can be overcome, as the technique solely probes molecular vibrations of inherent chemical structures of the sample which do not change in their intensity with time. According to fluorescence microscopy analysis, we imaged a TR146 cell layer by confocal Raman microscopy (alpha 300R+, WITec GmbH, Ulm, Germany) at an excitation wavelength of 532 nm (Nd:YAG laser operated at 30 mW before the objective). Raman spectra were collected through a Zeiss objective (63× magnification, NA = 1.0) at an integration time of 0.5 s. Image resolution was 0.5 μm × 0.5 μm.

The acquired spectral data set was background corrected and cosmic spikes were removed (software WITec Project Plus, WITec GmbH, Germany). Subsequently, the spectral data set was clustered. Here, each spectrum of the data set was sorted into one cluster according to the highlighted peaks of DNA and CH-vibrations in Fig. 1. Each cluster was allotted to a different colour and converted into a false colour Raman image (Fig. 2C). Image pixels assigned to Raman spectra of the cellular body are shown in red colour, whereas spectra acquired from the cell nuclei are depicted in blue image pixels. Based on the results of the cluster analysis, each component (nuclei and cell body) is depicted in a single Raman image (Fig. 2C, small panels), which can be overlaid for a combined visualization (Fig. 2C, large panel). Thus, despite the different procedures to generate microscopic images, the presentation of analytical results does not differ between confocal fluorescence and Raman microscopy proving the latter as a valuable technique for cellular investigations.

After successful label-free visualization of the model buccal epithelium, we performed confocal Raman microscopy to study the internalization of NM100 TiO_2 particles (TIONA) by buccal TR146 cells. Prior to uptake studies, TiO_2 particles dispersed in HBSS (10 μg ml^{-1}) were characterized. Hydrodynamic size, polydispersity index (PdI) and aggregation index (AI) were measured by photon correlation spectroscopy (Malvern ZetasizerNano ZSP, Malvern Instruments, UK) at a detection angle of 173°. The zeta potential was determined by laser Doppler velocimetry (scattering angle of 17°) coupled with photon correlation spectroscopy (Zetasizer SP, Malvern Instruments, Malvern, UK). The dispersed particles show a mean hydrodynamic size of 416.2 ± 50.65 nm and a zeta potential of −6.61 ± 2.27 mV, respectively. Furthermore, a PdI of 0.158 ± 0.059 and an aggregation index of −0.179 were measured. Consequently, as the PdI value is low, the TiO_2 particles form a stable suspension. Particles tend to form small

aggregates as the hydrodynamic size deviates from the nominated particle size of 125 nm. However, aggregates are uniform with smooth outer surface indicated by the low AI. These findings are in good agreement with electron microscopy studies performed on the TiO_2/HBSS dispersion (10 μg ml^{-1}) dried on a silicon wafer and sputter coated with gold. Images were taken with a Zeiss EVO HD15 electron microscope (Zeiss, Germany) at an accelerating voltage of 5 kV. Fig. 3A shows single TiO_2 particles as well as small aggregates within the size range nominated by PdI values.

Titanium dioxide exists in three polymorphs namely anatase, rutile, and brookite.[8,30] The NM100 TiO_2 (TIONA) particles are claimed to be anatase. To confirm this, we acquired a Raman spectrum of the raw material (ESI†). The identified Raman peaks at 146, 198, 398, 519, and 642 cm^{-1} are in good agreement with the peak positions for the Raman active modes of TiO_2 anatase crystals found in literature 144, 197, 639 cm^{-1} (all E_g), 399 cm^{-1} (B_{1g}) and 515 cm^{-1} (B_{1g} and A_{1g})[30–32] considering a resolution of 4 cm^{-1} of our spectrometer. Thus, the polymorphic form of TIONA particles used in our study is anatase.

The diverse spectral patterns of different cellular compartments facilitate not only the visualization of cells in detail by confocal Raman microscopy, but also revealing potential compartment specific internalization of particles in the cell. As tracing of particle uptake is based on spectral discrimination of the individual components, we first compared the single Raman spectra of the buccal cells and the TiO_2 model particles. Fig. 3B depicts the respective Raman spectra. The TiO_2 spectrum shows three outstanding peaks at 398, 519 and 642 cm^{-1} in the lower wavenumber region, whereas prominent peaks from cellular spectra are visible at higher wavenumbers (500–1800 cm^{-1}). Thus, spectral discrimination and consequently particle tracing is feasible by using the peak at 642 cm^{-1} for TiO_2 (Fig. 3B).

For particle uptake studies, TR146 cell layers were incubated with NM 100 TiO_2 (TIONA) particle suspension (10 μg ml^{-1} in HBSS) prior to Raman analysis. After 4 hours, residual particles were removed in three washing steps. Subsequently, samples were fixed and placed on the scan stage of the confocal microscope for Raman spectra acquisition. At first, Raman spectra from the lateral plane (*xy*) were recorded. The spectral data sets were background subtracted. Subsequently, cluster analysis was performed using the peaks at 642 cm^{-1} as well as the peaks at 785, 1095 and 1575 cm^{-1} to differentiate TiO_2 and cell nucleus from the cell body spectra. The resulting lateral image in Fig. 4A shows the location of TiO_2 particle agglomerates (yellow) on the cells. However, lateral images do not differentiate surface attached and internalized particles as they were only recorded

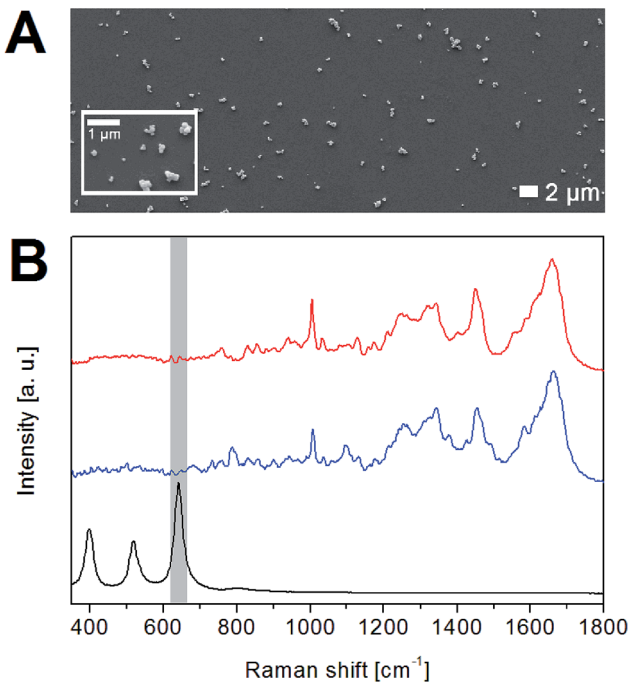

Fig. 3 (A) Electron microscopy image of TiO_2 particles. (B) Raman spectra of cellular compartments (red: cell body; blue: nucleus) and TiO_2 particles (black). The highlighted peak represents the peak used for TiO_2 identification.

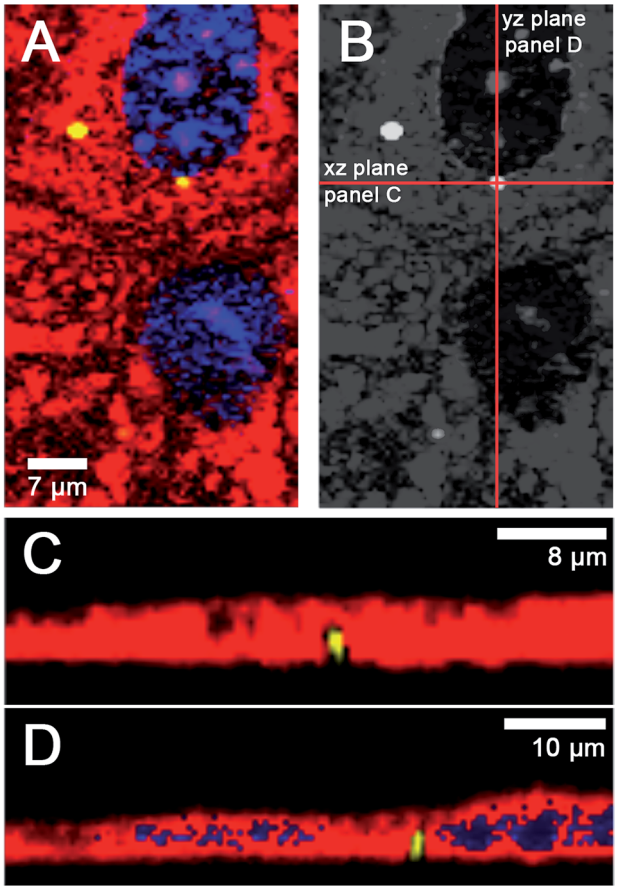

Fig. 4 Particle internalization study by confocal Raman microscopy. (A) Lateral false colour image showing the position of agglomerated TiO_2 particles (yellow) on the cell layer (nuclei in blue, cell body in red). (B) Decolourized panel A with red lines representing vertical planes for Raman microscopy analysis to discriminate between particle adhesion and internalization. (C) and (D) Raman microscopy cross section images showing internalized TiO_2 particles from the *xz*-plane (C) as well as from the *yz*-plane (D).

in one horizontal focal plane. Therefore, to prove internalization, additional cross section images are required.

Confocal Raman microscopy allows spectral acquisition in vertical as well as in horizontal planes. Thus, cross section images of cells can be acquired by virtually cutting through the cell. In Fig. 4B, the location of virtual planes exemplarily cutting the cell layer in vertical directions for Raman analysis is marked. Due to the non-destructive working principle of the analytical technique, the sample is investigated in its fixed state. As neither particles nor cellular compartments are labelled, interactions of TR146 cells with model TiO_2 particles are not altered and analytical results represent the actual native condition of the system. The acquired Raman spectra from vertical planes in *xz*- as well as in *yz*-direction, encompassing the localized TiO_2 particle, were converted into false colour Raman images. Both cross section images prove the cellular internalized TiO_2 as visualized in Fig. 4C (*xz*) and Fig. 4D (*yz*). Thus, oral buccal epithelia cells take up TiO_2 particles within 4 hours. With virtual cross sectioning, it can be differentiated between adhesion and internalization, not only with regards to the entire cell, but also within endogeneous cell compartments.

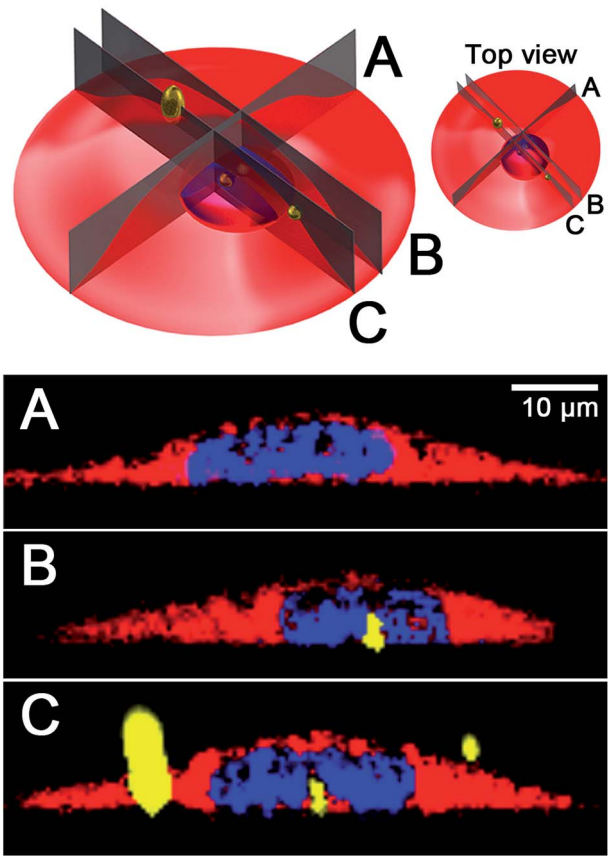

Fig. 5 Three dimensional sketch of a cell showing different particle engulfment states. Virtual vertical planes locating the area for confocal Raman microscopy are indicated. (A) Raman image showing a vertical plane set off target. (B) Raman image depicting a nucleus engulfed particle. (C) False colour cross section image visualizing multiple locations of particles on the cell. Cell bodies are shown in red, nuclei in blue and TiO_2 in yellow.

Therefore, label-free imaging in vertical planes with confocal Raman microscopy is beneficial for non-destructive observation of compartment specific particle internalization. Especially, particle invasion into the cell nucleus is of high interest, as this effect could potentially initiate genotoxic effects *in vivo*.

In this study, multiple areas of at least three incubated different cell layers were investigated. In all analyzed samples, various locations of internalized TiO_2 within cells were determined, even the enclosure of TIONA particles into the nucleus as a distinct cellular compartment was detected. Here, the gain of non-destructive cross section Raman imaging becomes evident. A three dimensional cell sketch depicting particles in different engulfment states is shown in Fig. 5, revealing that the selection of the right analysis plane is of high importance. The individual virtual section planes *A*, *B* and *C* represent different positions to localize particles as shown in their respective Raman images in the lower panel A, B and C. Fig. 5A solely depicts cell body and nucleus, whereas in the appropriate vertical plane particles can be localized within the nucleus due to spectral discrimination (Fig. 5B). Even cell adhesive and nucleus ingested particles can simultaneously be displayed in one image (Fig. 5C). However, to state and prove possible effects such as genotoxic consequences of the TiO_2 invasion into the nucleus, a subsequent, profound analysis on the molecular level and *in vivo* studies have to follow.

Conclusions

In this study, we successfully performed confocal Raman microscopy to image buccal epithelial cells on a subcellular level by discriminating between spectral differences of cell body and nucleus. The false colour Raman images were compared with fluorescence microscopy images. Coinciding analytical results prove confocal Raman microscopy to be a suitable complimentary label-free technique.

Furthermore, the internalization of TiO_2 particles into oral buccal epithelial cells was visualized in lateral images as well as in virtual cross section images. Here, analysis benefits from the chemically selective operating principle of confocal Raman microscopy as the samples are not altered for investigation. Based on non-destructive cross sectional imaging, differentiation between particle adhesion and internalization is enabled. Additionally, particle invasion into the cell nucleus was visualized. Thus, confocal Raman spectroscopy shows a high potential as a valuable method to follow selective particle uptake into endogenous cell compartments as the nucleus.

Overall, further studies of epithelial cell culture models and particle interaction can benefit from three dimensional confocal Raman microscopy analyses, circumventing the necessity of laborious sample preparation without losing analytical accuracy.

Acknowledgements

The authors thank C. Stiers for creating schematic graphs of the cell, B. Bauer for helping with the cell culture experiments and

and M. Absenger for the support in acquisition of confocal fluorescence microscopy images.

Notes and references

1 M. C. Lomer, R. P. Thompson, J. Commisso, C. L. Keen and J. J. Powell, *Analyst*, 2000, **125**, 2339–2343.
2 M. C. Lomer, C. Hutchinson, S. Volkert, S. M. Greenfield, A. Catterall, R. P. Thompson and J. J. Powell, *Br. J. Nutr.*, 2004, **92**, 947–955.
3 ICTA, *Petition to the United States Food and Drug Administration*, 2006.
4 A. T. Harris and R. Bali, *J. Nanopart. Res.*, 2008, **10**, 691–695.
5 F. Gottschalk, T. Sonderer, R. W. Scholz and B. Nowack, *Environ. Sci. Technol.*, 2009, **43**, 9216–9222.
6 D. P. K. Lankveld, A. G. Oomen, P. Krystek, A. Neigh, A. Troost de Jong, C. W. Noorlander, J. C. H. Van Eijkeren, R. E. Geertsma and W. H. De Jong, *Biomaterials*, 2010, **31**, 8350–8361.
7 J. J. Powell, N. Faria, E. Thomas-McKay and L. C. Pele, *J. Autoimmun.*, 2010, **34**, J226–J233.
8 E. Fröhlich, B. J. Teubl and E. Roblegg, *Bionanomater. Dent. Appl.*, 2013, **14**, 25–35.
9 OECD, in *Chemicals Testing Monographs No. 29*, 2011.
10 C. A. Lesch, C. A. Squier, A. Cruchley, D. M. Williams and P. Speight, *J. Dent. Res.*, 1989, **68**, 1345–1349.
11 H. Zhang and J. R. Robinson, in *Oral Mucosal Drug Delivery*, ed. M. J. Rathbone, Marcel Dekker, New York, 1996, pp. 51–63.
12 J. Jacobsen, B. Vandeurs, M. Pedersen and M. R. Rassing, *Int. J. Pharm.*, 1995, **125**, 165–184.
13 E. Roblegg, E. Frohlich, C. Meindl, B. Teubl, M. Zaversky and A. Zimmer, *Nanotoxicology*, 2012, **6**, 399–413.
14 B. J. Teubl, M. Absenger, E. Fröhlich, G. Leitinger, A. Zimmer and E. Roblegg, *Eur. J. Pharm. Biopharm.*, 2013, **84**, 386–393.
15 A. Nijssen, T. C. B. Schut, F. Heule, P. J. Caspers, D. P. Hayes, M. H. A. Neumann and G. J. Puppels, *J. Invest. Dermatol.*, 2002, **119**, 64–69.
16 N. J. Crane, T. S. Brown, K. N. Evans, J. S. Hawksworth, S. Hussey, D. K. Tadaki and E. A. Elster, *Wound Repair Regen.*, 2010, **18**, 409–416.
17 B. Brozek-Pluska, J. Musial, R. Kordek, E. Bailo, T. Dieing and H. Abramczyk, *Analyst*, 2012, **137**, 3773–3780.
18 L. Mavarani, D. Petersen, S. F. El-Mashtoly, A. Mosig, A. Tannapfel, C. Koetting and K. Gerwert, *Analyst*, 2013, **138**, 4035–4039.
19 C. Matthaus, T. Chernenko, J. A. Newmark, C. M. Warner and M. Diem, *Biophys. J.*, 2007, **93**, 668–673.
20 K. Meister, D. A. Schmidt, E. Brundermann and M. Havenith, *Analyst*, 2010, **135**, 1370–1374.
21 A. A. van Apeldoorn, H. J. van Manen, J. M. Bezemer, J. D. de Bruijn, C. A. van Blitterswijk and C. Otto, *J. Am. Chem. Soc.*, 2004, **126**, 13226–13227.
22 C. Matthaeus, A. Kale, T. Chernenko, V. Torchilin and M. Diem, *Mol. Pharmaceutics*, 2008, **5**, 287–293.
23 T. Chernenko, C. Matthaus, L. Milane, L. Quintero, M. Amiji and M. Diem, *ACS Nano*, 2009, **3**, 3552–3559.
24 K. Meister, J. Niesel, U. Schatzschneider, N. Metzler-Nolte, D. A. Schmidt and M. Havenith, *Angew. Chem., Int. Ed.*, 2010, **49**, 3310–3312.
25 T. Chernenko, R. R. Sawant, M. Miljkovic, L. Quintero, M. Diem and V. Torchilin, *Mol. Pharmaceutics*, 2012, **9**, 930–936.
26 C. Matthäus, S. Schubert, M. Schmitt, C. Krafft, B. Dietzek, U. S. Schubert and J. Popp, *ChemPhysChem*, 2013, **14**, 155–161.
27 M. Diem, C. Matthäus, T. Chernenko, M. J. Romeo, M. Milkovic, B. Bird, J. Schubert, K. Papamarkakis and N. Laver, in *Infrared and Raman Spectroscopy Imaging*, ed. R. Salzer and H. W. Siesler, Wiley-VCH, Weinheim, 1st edn, 2009, ch. 5, pp. 173–201.
28 C. Krafft, T. Knetschke, R. H. W. Funk and R. Salzer, *Anal. Chem.*, 2006, **78**, 4424–4429.
29 K. T. Thurn, T. Paunesku, A. Wu, E. M. B. Brown, B. Lai, S. Vogt, J. Maser, M. Aslam, V. Dravid, R. Bergan and G. E. Woloschak, *Small*, 2009, **5**, 1318–1325.
30 T. Ohsaka, F. Izumi and Y. Fujiki, *J. Raman Spectrosc.*, 1978, **7**, 321–324.
31 V. Swamy, A. Kuznetsov, L. S. Dubrovinsky, R. A. Caruso, D. G. Shchukin and B. C. Muddle, *Phys. Rev. B: Condens. Matter Mater. Phys.*, 2005, **71**, 184302.
32 J. Surmacki, P. Wronski, M. Szadkowska-Nicze and H. Abramczyk, *Chem. Phys. Lett.*, 2013, **566**, 54–59.

